Digital magnetic moment of tetrahedrally bonded half-metallic nanoclusters

Masao Nakao*

Department of Precision Engineering, Tokai University, 1117 Kitakaname, Hiratsuka, Kanagawa 259-1292, Japan
(Received 27 January 2004; revised manuscript received 6 April 2004; published 28 June 2004)

We investigate the half metallicity and localized spin magnetic moments for individual nanoclusters of zinc-blende transition-metal pnictides and chalcogenides TX (T=V, Cr, and Mn; X=N, P, As, Sb, S, Se, and Te) using first-principles molecular-orbital calculations. These nanoclusters, as well as the bulk, show half-metallic ferromagnetic behavior for a wide range of bond lengths; otherwise, an antiferromagnetic arrangement is stabilized. The total magnetic moment of an isolated half-metallic nanocluster $T_k X_\ell$ turns out to be $(Z_{tot} - 8)k + (4 - \Delta Z)(k - \ell)$ in units of μ_B, where Z_{tot} is the total number of valence electrons per formula unit, $\Delta Z = 1$ for pnictides, and $\Delta Z = 2$ for chalcogenides. This ℓ dependence results from anion dangling hybrids on the cluster surface. Induced antiparallel magnetic moments at anion sites are interpreted in terms of a bond-orbital model; the hybridization effect between cation d states and anion p states creates holes in the majority-spin states of the bond orbitals. When the nanocluster is embedded in a lattice-matched compound semiconductor with a common anion, the total moment approaches $(Z_{tot} - 8)k \mu_B$. Half metallicity is maintained at the boundary sites of the nanocluster without any sign of interface states, suggesting the Ohmic nature of the contact.

I. INTRODUCTION

For future spin electronics or *spintronics*,[1–4] where it is not only the electron charge but the electron spin that carries information, it is essential to inject spins from highly spin-polarized ferromagnets into nonmagnetic semiconductors. In contrast to the giant magnetoresistance (GMR) in metallic magnetic multilayers,[5,6] semiconductor-based transport offers various advantages over metals such as a long spin lifetime[7] and persistent spin coherence.[8] So far, spin-polarized hole injection from diluted magnetic semiconductors (DMS's) to III-V and II-VI semiconductors has already been demonstrated,[9,10] whereas the spin injection from metallic ferromagnets has only recently been realized by introducing tunnel barriers including Schottky contacts,[11–13] thin metal oxides,[14,15] and AlAs.[16] In the most promising Mn-doped GaAs, however, the Curie temperature T_C is as low as 110 K due to the limited solubility of Mn in GaAs.[17]

Half metals (HM's) have received considerable interest in recent years because of the complete polarization of carriers.[18] In these materials, one spin channel is metallic while the other is insulating. After de Groot *et al.*[19] initially predicted the half-metallic behavior of $C1_b$-type Heusler alloys, NiMnSb and PtMnSb, such a behavior was found in various perovskite structures[20,21] and rutile-structured CrO_2.[21–23] Although these oxides were proved practically 100% spin polarized,[20,21] besides their low T_C, the stoichiometry of oxides is difficult to control and defects limit coherent carrier transport.

A new class of prospective HM's is zinc-blende (ZB) transition-metal pnictides and chalcogenides, which are compatible with ordinary III-V and II-VI semiconductors. Since the initial prediction and subsequent synthesis of ZB CrAs,[24] several band-structure calculations have appeared.[25–38] As these compounds can be viewed as the 100% doping limit of DMS's, they are generally metastable in the ZB structure. In the bulk, they crystallize in either the hexagonal NiAs or the orthorhombic MnP structure as the ground state. The stable

NiAs phase is a metallic ferromagnet or an antiferromagnet but show no gap.[28,31,32,37,38] Recent molecular-beam-epitaxy (MBE) techniques, however, enable us to grow the ZB phase of CrAs (Refs. 24 and 39), MnAs (Ref. 40), and CrSb (Ref. 41) in the form of thin films, nanodots, and multilayers such as CrAs/GaAs (Ref. 39) and CrSb/GaAs (Ref. 42). A fundamental question arises whether such nanostructures (individual nanostructures and/or nanostructured materials) present half-metallic behaviors as well as the bulk materials or conversely what is the essential difference between the nanostructures and the bulk materials.

The purpose of this paper is to investigate theoretically the electronic structures for tetrahedrally coordinated nanoclusters of transition-metal pnictides and chalcogenides TX (T=V, Cr, and Mn; X=N, P, As, Sb, S, Se, and Te) by means of first-principles molecular-orbital methods. In Sec. II, we focus on the half metallicity of a CrAs nanocluster and its Cr-As bonding nature. The computational results are interpreted in terms of the bond-orbital model (BOM), a simplified model based on a linear-combination-of-atomic-orbitals (LCAO) method, proposed by Harrison.[43,44] In Sec. III, we reformulate the BOM theory, taking into account the hybridization effect between transition-metal d states and the bond orbitals. We call it "ghost-bond-orbital model." Applying the BOM picture to an individual nanocluster, we demonstrate that the total spin magnetic moment is an exact integer when the nanocluster shows half metallicity. In Sec. IV, the integer magnetic moments and the stability of ferromagnetic states are confirmed numerically in the series of TX nanoclusters for various bond lengths. Then, in Sec. V, we discuss the trend in the bond properties such as polarity and hole density with bond length to justify the validity of BOM. In Sec. VI, we treat the CrAs nanocluster embedded in a lattice-matched GaAs matrix. Section VII contains concluding remarks.

II. HALF METALLICITY

Our approach is based on the DV-$X\alpha$ method[45,46] that utilizes discrete-variational (DV) integral and local-density
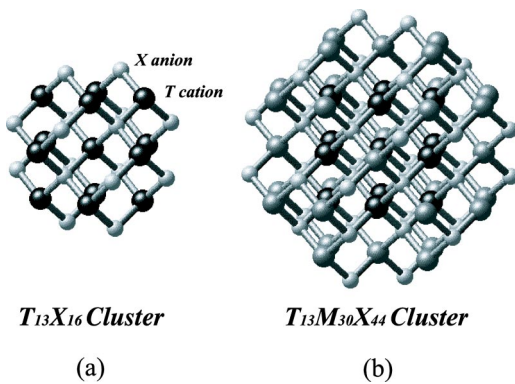
FIG. 1. Cluster models employed in the DV-$X\alpha$ calculation. (a) $T_{13}X_{16}$ cluster of zinc-blende transition-metal pnictides and chalcogenides with $T=$V, Cr, and Mn and $X=$N, P, As, Sb, S, Se, and Te. (b) $T_{13}M_{30}X_{44}$ cluster: The $T_{13}X_{16}$ cluster is embedded in an MX matrix.

approximation ($X\alpha$) with $\alpha=0.7$.[50] The Hamiltonian and overlap matrices of a variational expansion of eigenfunctions are calculated in a numerical atomic orbital basis by a numerical integration procedure with a weighted sum over a set of sample points. In our calculations, 500 sample points per atom are used. The basis functions are obtained from numerical solutions of cations and anions in the crystal field of the given cluster model. Such a basis provides a compact and efficient set of expansion functions which can be systematically refined during the self-consistent process as needed. Unlike the band-structure calculations including the LCAO method, the periodicity of crystal lattices is not essential for this approach. As shown in Fig. 1(a), the cluster model employed in this study is considered to be the smallest theoretical nanoparticle displaying the same T_d symmetry as the ZB bulk crystal. The $T_{13}X_{16}$ cluster consists of a central TX_4 "core" and its nearest-neighbor $T_{12}X_{12}$ "shell." Positions of the atoms remain the same as in the bulk crystal. The $T_{13}M_{30}X_{44}$ cluster in Fig. 1(b) represents the $T_{13}X_{16}$ cluster embedded in a lattice-matched MX compound semiconductor with a common nonmetallic X constituent.

Figure 2 presents the spin-resolved total and partial densities of states (DOS's) for a $Cr_{13}As_{16}$ cluster, which are averaged separately at the central core sites [Fig. 2(a)] and the surrounding shell sites [Fig. 2(b)] using the GaAs bond length of 0.245 nm. The ZB CrAs is the most extensively studied member of the TX compounds and its predicted equilibrium lattice constant is compatible with those of GaAs and AlAs for heteroepitaxy.[36] Self-consistent calculations are carried out in terms of T_d-symmetric molecular orbitals. Although the nanocluster is analogous to a molecule having discrete energy levels with bonding and antibonding orbitals, it is convenient to convert a set of energy levels into a continuous DOS curve by the Gaussian broadening. Clearly, the CrAs nanocluster shows a half-metallic electronic structure; the majority-spin channel is metallic while the minority-spin channel is insulating.

In the tetrahedral environment, the transition-metal d states are split into a doubly degenerated e_g state and a triply degenerated t_{2g} state; the e_g state is lower in energy than the
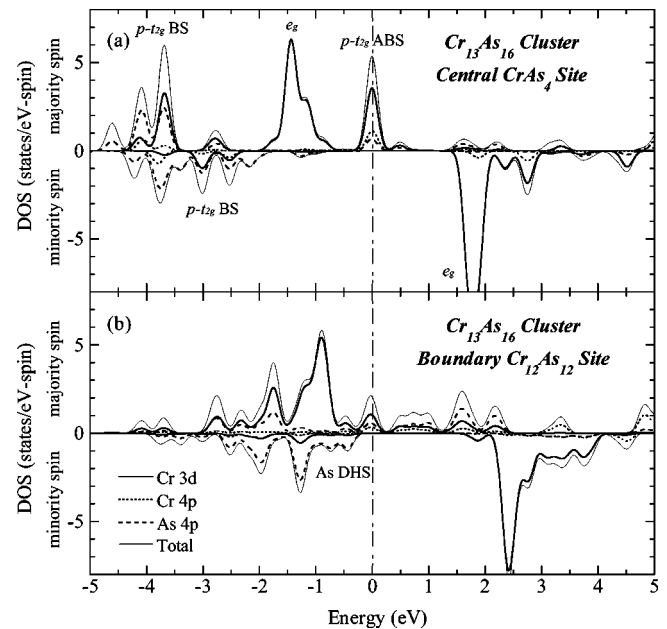
FIG. 2. Spin-resolved total and partial densities of states (DOS's) for a $Cr_{13}As_{16}$ cluster averaged at (a) central $CrAs_4$ sites and (b) surrounding $Cr_{12}As_{12}$ sites using the GaAs bond length $d_{GaAs}=0.245$ nm. The energy levels are broadened by Gaussians with a half width of 0.1 eV.

t_{2g} state. Since the p states of the four neighboring nonmetallic atoms have the same t_{2g} symmetry, the t_{2g} states hybridize strongly with the p states. As indicated in Fig. 2(a), the symmetry-induced p-d hybridization forms a lower p-t_{2g} bonding state (BS) with As $4p$ character and a higher p-t_{2g} antibonding state (ABS) with Cr $3d$ character. In contrast, the hybridization between the e_g states and the p states is weak (but not zero in a finite cluster) due to symmetry, so that the e_g state is nonbonding in nature.

According to the BOM description, bond orbitals are formed for all the inner bonds in an individual cluster, but those sp^3 hybrid orbitals directed out of the cluster surface remain unbonded. There exist two types of *dangling hybrids* on the surface of the $Cr_{13}As_{16}$ cluster; generally, the dangling hybrids associated with nonmetallic atoms will have lower energies than those associated with transition-metal atoms. In fact, the As dangling hybrid states [DHS, labeled by As DHS in Fig. 2(b)] are fully occupied, whereas the Cr ones that not appear within the minority-spin gap are empty.

The overlap population diagram given in Fig. 3 helps us understand the nature of bonding in CrAs. As seen in Fig. 3(a), the bonding inside the $Cr_{13}As_{16}$ cluster is typically covalent. Thus, it is quite natural to pick four sp^3 hybrids instead of atomic orbitals in making the BOM approximation. Comparing their peak positions with the orbital-resolved partial density of states (PDOS) calculated at the central Cr and As sites in Fig. 3(b), we notice that the combination of Cr $3d$, $4p$ and As $4p$ states is responsible for the bonding in both majority- and minority-spin states. Evidently, d electrons also participate in the Cr-As covalent bonding.

On the other hand, we also notice that the antibonding states formed by the coupling of the Cr d states and the
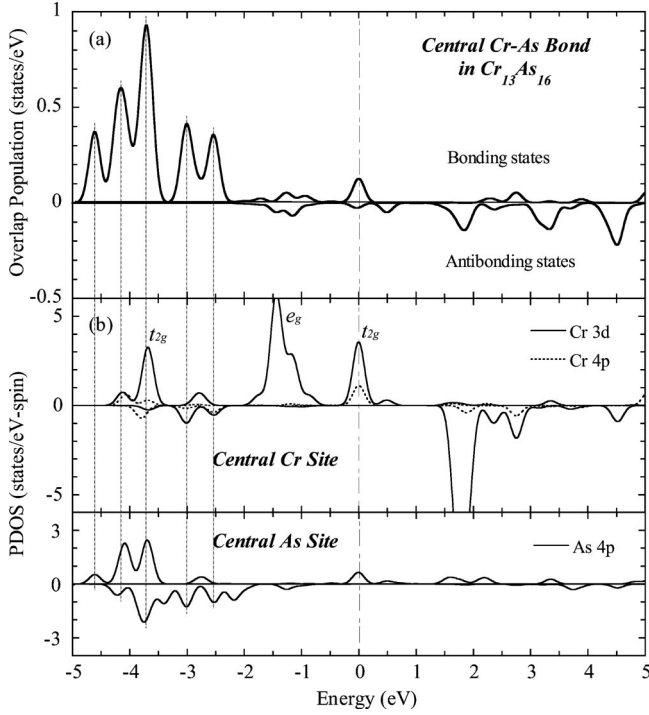
FIG. 3. (a) Overlap population diagram for the central Cr-As bond in a $Cr_{13}As_{16}$ cluster using the GaAs bond length d_{GaAs} =0.245 nm, which is compared with (b) partial density of states (PDOS) calculated at the central Cr and As sites in Fig. 2. The energy levels are broadened by Gaussians with a half width of 0.1 eV.

As sp^3 hybrids are present below the Fermi energy E_F. Since both bonding and antibonding states due to the weak coupling with the e_g states are occupied, the nonbonding e_g states, indeed, do not have any effect on the bonding properties. At E_F, the bonding states of the Cr and As sp^3 hybrids are more dominant than the p-t_{2g} antibonding states. It is a consequence of the electron transfer from the As sp^3 hybrids to the Cr $3d$ states that a d electron well localized at the Cr site leaves one bond orbital made up of the sp^3 hybrids empty. This electron transfer will explain the origin of induced magnetic moments at As sites.

III. GHOST-BOND-ORBITAL MODEL

In usual band-structure calculations, the charge to be associated with an atom is an ill-defined quantity because there is arbitrariness in associating each contribution of the charge density to a particular atom or a particular bond. However, the choice becomes quite natural within the framework of the LCAO model. In particular, the excess number of electrons placed on the anion from each bond is called *polarity* in BOM.

A. Polarity and hole density

For ZB half metals, we may expect the formation of a strong sp^3 bond just like the ordinary III-V and II-VI compound semiconductors.[28] We shall modify BOM to include

the d orbitals of transition metals. The first step in the formation of bond orbitals is the construction of sp^3 hybrid orbitals, $|a\rangle$ on the anion and $|c\rangle$ on the cation. Of course, the transition metal is the cation and the group-V or group-VI element is the anion. The hybrid energy on the anion is given by

$$\epsilon^A \equiv \langle a|\hat{H}|a\rangle = \frac{1}{4}(\epsilon_s^A + 3\epsilon_p^A), \tag{1}$$

where ϵ_s^A and ϵ_p^A are s- and p-state energies of the anion, respectively. Setting aside the d states for the moment, we also define the corresponding energy ϵ^C on the cation. The *polar energy* is half the energy change in transferring an electron from anion to cation,

$$V_3 = \frac{1}{2}(\epsilon^C - \epsilon^A). \tag{2}$$

Since such hybrids are not eigenstates, there are nonzero matrix elements of the Hamiltonian between the hybrids. The *covalent energy*, the matrix element between two hybrids extending into the same bond, is written

$$V_2 \equiv -\langle c|\hat{H}|a\rangle. \tag{3}$$

Although these two hybrids are not orthogonal to each other, the overlap $\langle c|a\rangle$ can be absorbed in a readjustment of the covalent and polar energies.[44,47] We now transform pairs of hybrid orbitals in each bond into bonding and antibonding states. By minimizing the bond energy of a linear combination of two hybrids within each bond, we obtain a bond orbital

$$|b\rangle = \left[\frac{1}{2}(1 + \alpha_p)\right]^{1/2}|a\rangle + \left[\frac{1}{2}(1 - \alpha_p)\right]^{1/2}|c\rangle, \tag{4}$$

where the polarity α_p is defined as

$$\alpha_p = V_3/(V_2^2 + V_3^2)^{1/2}. \tag{5}$$

The *bond energy*, the expectation value of the Hamiltonian with respect to this bond orbital, is given by

$$\langle b|\hat{H}|b\rangle = \frac{1}{2}(\epsilon^A + \epsilon^C) - (V_2^2 + V_3^2)^{1/2}. \tag{6}$$

The bond orbital can accommodate two electrons (one per spin), so each bonds contribute $1 + \alpha_p$ electrons to the anion and $1 - \alpha_p$ electrons to the cation.

One possible way to take account of the p-d hybridization effect is the incorporation of the t_{2g} state into the linear combination to make up the bond orbital. We might imagine making the corresponding unitary transformation on the states, obtaining bonding and antibonding combinations of the t_{2g} state and the surrounding bond orbitals. This procedure is quite similar to the construction of the original bond orbital. Let us call these bonding states including the t_{2g} component as *ghost bond orbitals* (GBO's). The hybridization effect depends strongly on the energy separation between the t_{2g} state and the bond energy in Eq. (6). For minority-spin electrons, we can practically neglect the effect at least for electron counting, because the two states are
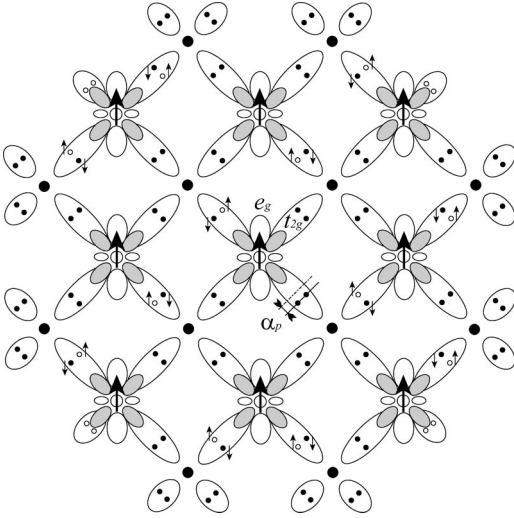
FIG. 4. Schematic ghost-bond-orbital model for $T_{13}X_{16}$ clusters viewed in the [100] direction. The open circles represent transition-metal atoms (cations) with t_{2g} and e_g orbitals; the neighboring black circles are anions. The black and open dots within the ovals represent electrons and holes in the bond orbitals, respectively.

separated by a wide energy gap due to the exchange splitting. As for majority-spin electrons, the modification is most simply calculated by returning to one bond orbital and calculating the charge that is transferred to the transition-metal d states. We now regard the d states simply as localized "electron reservoirs" and GBO's as bond orbitals containing holes. Instead of evaluating the Hamiltonian matrix elements, we will fit the polarity to reproduce the self-consistent magnetic moments calculated with the DV-$X\alpha$ method.

The schematic ghost-bond-orbital model for the $T_{13}X_{16}$ clusters viewed in the [100] direction is illustrated in Fig. 4. The open circles represent transition-metal atoms (cations) with t_{2g} and e_g orbitals; then the neighboring black circles are nonmetallic atoms (anions). The black and open dots within the ovals represent electrons and holes in the bond orbitals, respectively. On the surface of the cluster, the anion dangling hybrids are fully occupied, while the cation ones are empty. The presence of holes in the majority-spin states of the anion dangling hybrids is also possible, but do not affect the total magnetic moments. The majority-spin electron that create a hole in the dangling hybrid moves to the d state of the cation.

B. Spin magnetic moments

We shall, for the moment, confine ourselves to the electron counting for estimating localized magnetic moments. The electron transfer from the anion hybrids to the d states introduces holes into the bond orbitals, thus modifying the polarity α_p of the bond. Each anion in a tetrahedral structure contains a net charge (in units of $-e$) of

$$Z^{*A} = -Z^{*C} = 4\alpha_p - 2n_h(1 + \alpha_p) - \Delta Z, \tag{7}$$

where n_h is the hole density of the bond orbital and ΔZ is the difference in valence from 4 (i.e., $\Delta Z = 1$ for group-V ele-

ments and $\Delta Z = 2$ for group-VI elements). In half-metallic states, the minority gap at E_F leaves the minority GBO's fully occupied and all higher minority-spin states empty, giving a total minority occupation of 4. This electron counting yields an integer total magnetic moment of $(Z_{tot} - 8)\mu_B$, where Z_{tot} is the total number of valence electrons per formula unit.[34] As for the majority-spin electrons, the introduction of holes into the bond orbitals must be considered.

We write anion and cation magnetic moments

$$m^A = m_{sp}^A, \tag{8a}$$

$$m^C = m_{sp}^C + m_d^C = (Z_{tot} - 8)\mu_B - m_{sp}^A. \tag{8b}$$

Once electrons transfer from the surrounding bond orbitals to the d state, the holes left behind will produce a negative magnetic moment opposite to the total moment. In the context of BOM, the natural choice is to associate a fraction $(1 + \alpha_p)/2$ of the n_h holes per bond with the anion and a fraction $(1 - \alpha_p)/2$ with the cation. Their sp and d components are then given by

$$m_{sp}^A = -2n_h(1 + \alpha_p)\mu_B, \tag{9a}$$

$$m_{sp}^C = -2n_h(1 - \alpha_p)\mu_B, \tag{9b}$$

$$m_d^C = (Z_{tot} - 8 + 4n_h)\mu_B. \tag{9c}$$

To fit the values of α_p and n_h with DV-$X\alpha$ calculations, combining Eqs. (7) and (9a), we obtain

$$\alpha_p = \frac{1}{4}(\Delta Z + Z^{*A} - m^A/\mu_B), \tag{10}$$

and

$$n_h = \frac{-m^A}{2(1 + \alpha_p)\mu_B} = \frac{-2m^A}{(4 + \Delta Z + Z^{*A})\mu_B - m^A}. \tag{11}$$

C. BOM analysis for nanoclusters

In nanoclusters, a local net charge associated with each atom depends on its local environment for lack of periodicity. Thus, unlike the bulk, there is no unique polarity defined. For the central bond, connecting between the central (0th) cation site and the first-nearest-neighbor anion site, the local polarity is given by

$$\alpha_p^{0,1} = \frac{1}{4}(\Delta Z - Z_0^{*C} + m_0^C/\mu_B - Z_{tot} + 8) \tag{12}$$

instead of Eq. (10). The local hole density in Eq. (11) becomes

$$n_h^{0,1} = \frac{m_0^C - (Z_{tot} - 8)\mu_B}{2(1 + \alpha_p^{0,1})\mu_B}. \tag{13}$$

Similarly, for the next bond between the first- and the second-nearest-neighbor sites, we obtain

TABLE I. Total spin magnetic moment of the $T_{13}X_{16}$ (X is a group-V element) cluster in μ_B calculated using the bond lengths of several ZB III-V semiconductors. Integer magnetic moments (17, 30, and 43) indicate that the cluster is half metallic. A negative value corresponds to an antiferromagnetic spin arrangement. For each compound, the equilibrium bond length predicted for the bulk system is given in parentheses, and the moments are underlined for the bond lengths within 4% of equilibrium.

d(nm) Compound	d_{InN} 0.216	d_{GaP} 0.236	d_{GaAs} 0.245	d_{InP} 0.253	d_{InAs} 0.262	d_{GaSb} 0.264	d_{InSb} 0.280
VN (0.182)[a]	17	17	−13.01	−13	−13	−12.99	17
VP (0.228)[a]	0.68	17	17	17	−13.24	−13.22	17
VAs (0.234)[a]	17	17	17	17.02	17.13	17.12	17
VSb (0.259)[a]	17	17	17.01	18.65	21.97	22.21	22.58
CrN (0.177)[a]	30	30	30	30	30	30	30
CrP (0.232)[b]	30	30	30	30	30	30	30
CrAs (0.246)[b]	30	30	30	30	30	30	30
CrSb (0.266)[b]	30	30.39	31.53	32.42	31.64	31.41	30
MnN (0.176)[a]	−33	−33	-33	−33	−33	−33	43
MnP (0.217)[a]	−33	−33	43	43	43	43	43
MnAs (0.248)[b]	−33	39	43	43	43	43	43
MnSb (0.268)[b]	−33	43	43	43	43	43	43

[a]Reference 34.
[b]Reference 36.

$$\alpha_p^{1,2} = \frac{1}{4}\left\{\Delta Z + \frac{1}{3}(4Z_1^{*A} + Z_0^{*C}) - \frac{1}{3}[4m_1^A/\mu_B \right.$$
$$\left. + 2n_h^{0,1}(1 + \alpha_p^{0,1})]\right\}, \qquad (14)$$

and

$$n_h^{1,2} = \frac{-4m_1^A - 2n_h^{0,1}(1 + \alpha_p^{0,1})\mu_B}{6(1 + \alpha_p^{1,2})\mu_B}. \qquad (15)$$

On the surface of the $T_{13}X_{16}$ cluster, since a couple of dangling hybrids are fully occupied at the anion sites (see Fig. 4), we have

$$\alpha_p^{2,3} = \frac{1}{2}(\Delta Z - 2 + Z_3^{*A} - m_3^A/\mu_B) \qquad (16)$$

and

$$n_h^{2,3} = \frac{-m_3^A}{(1 + \alpha_p^{2,3})\mu_B}. \qquad (17)$$

The total spin magnetic moment of the cluster M_{tot} is evaluated simply by summing up all the local moments: m_0^C, m_1^A, m_2^C and m_3^A. Here

$$m_2^C = Z_{tot} - 8 - \frac{1}{4}(4 - \Delta Z) + \frac{1}{2}n_h^{1,2}(1 + \alpha_p^{1,2}) + n_h^{2,3}(1 + \alpha_p^{2,3}). \qquad (18)$$

Using the charge neutrality condition of the cluster, we find

$$M_{tot}(T_{13}X_{16}) = [13(Z_{tot} - 8) - 3(4 - \Delta Z)]\mu_B. \qquad (19)$$

The generalization of this expression for an arbitrary cluster $T_k X_\ell$ leads to

$$M_{tot}(T_k X_\ell) = [(Z_{tot} - 8)k + (4 - \Delta Z)(k - \ell)]\mu_B. \qquad (20)$$

Note that the integer total magnetic moment depends not only on the number of transition-metal atoms k but also on that of nonmetallic atoms ℓ. This is not surprising because an anion dangling hybrid (fully occupied) removes $(4 - \Delta Z)/4$ electrons from the majority d states, exhibiting no magnetic moment; conversely, a cation dangling hybrid (empty) contributes $(4 - \Delta Z)/4$ electrons to the majority d states. On the average, the total magnetic moment per formula unit, $m^A + m^C = (Z_{tot} - 8)\mu_B$, predicted for the bulk is valid only when $k = \ell$.

IV. TOTAL MAGNETIC MOMENT

To estimate the orbital occupations of the $T_{13}X_{16}$ clusters numerically, we perform the Mülliken population analysis,[48,49] which is a convenient way to separate different contributions to the total charge density. Now, we start DV-$X\alpha$ calculations under the initial condition that only the central transition-metal atom is a high-spin (spin-up) state and the others are nonmagnetic states. Prior to the self-consistent calculations, it is unpredictable in which state the result converges, ferromagnetic, antiferromagnetic, or nonmagnetic.

Using the bond lengths of several ZB III-V semiconductors, we list the calculated total spin magnetic moments for the $T_{13}X_{16}$ clusters with a group-V element as X in Table I. Obviously, integer magnetic moments (17, 30, and 43) indicate that the cluster is half metallic. A negative value corresponds to an antiferromagnetic spin arrangement where the surrounding twelve T atoms have spin-down states as opposed to the spin-up state at the central site. This arrangement is, of course, unfavorable in the bulk crystal in light of periodicity. Table II contains the total spin magnetic mo-

TABLE II. Total spin magnetic moment of the $T_{13}X_{16}$ (X is a group-VI element) cluster in μ_B calculated using the bond lengths of several ZB II-VI semiconductors. Integer magnetic moments (33, 46, and 59) indicate that the cluster is half metallic. A negative value corresponds to an antiferromagnetic spin arrangement. For each compound, the equilibrium bond length predicted for the bulk system is given in parentheses, and the moments are underlined for the bond lengths within 4% of equilibrium.

d(nm) Compound	d_{ZnS} 0.234	d_{ZnSe} 0.245	d_{CdS} 0.252	d_{CdSe} 0.262	d_{ZnTe} 0.263	d_{CdTe} 0.281
VS (0.227)[a]	$\underline{-30.60}$	-27.03	33	33	33	-26.92
VSe (0.241)[a]	$\underline{33}$	$\underline{33}$	33	33	33	33
VTe (0.272)[b]	33	33	33	$\underline{33}$	$\underline{33}$	$\underline{33}$
CrS (0.218)[a]	-36.09	46	46	46	46	46
CrSe (0.253)[b]	46	$\underline{46}$	$\underline{46}$	$\underline{46}$	46	46
CrTe (0.273)[b]	-36.34	46	46	46	$\underline{46}$	$\underline{46}$
MnS (0.212) [a]	-49	59	59	-49	-49	-49
MnSe (0.245)[a]	59	$\underline{59}$	-49	-49	-49	-49
MnTe (0.264)[a]	-49	59	59	$\underline{59}$	$\underline{59}$	-49

[a]Reference 34.
[b]Reference 38.

ments for the $T_{13}X_{16}$ clusters with a group-VI element as X calculated using the bond lengths of several ZB II-VI semiconductors. Similarly, integer magnetic moments (33, 46, and 59) demonstrate their half metallicity.

Several important aspects can be pointed out from Tables I and II. The total magnetic moments given in Eq. (19) are valid for all the TX compounds investigated here. Noninteger magnetic moments larger than the value of Eq. (19) suggest that the Fermi energy is below the gap in the minority-spin channel, passing through the anion DHS's. More specifically, the electron transfer from these minority DHS's to the majority d states generates extra magnetic moments at the cation sites of the cluster surface. This situation can be seen in VAs, VSb, and CrSb. We can apply this criterion to a wide variety of nanoclusters regardless of the size and shape of the cluster being considered.

It is interesting to note that the antiferromagnetic clusters also exhibit integer magnetic moments especially in Mn-based compounds. The self-consistent result for the $Mn_{13}P_{16}$ cluster converges in an antiferromagnetic state when the bond length is smaller than the GaAs value. As typically shown in Fig. 5, the spin-down channel has an energy gap at E_F throughout the cluster; accordingly, the $Mn_{13}P_{16}$ cluster behaves like an "antiferromagnetic half metal." Here, we choose the initial spin state of the central Mn atom such that the spin direction of the surrounding Mn atoms becomes up for comparison with the ferromagnetic arrangement. Thus, the majority spin is down at the central core sites [Fig. 5(a)] but up at the surrounding shell sites [Fig. 5(b)]. Since the central moment reverses direction compared with the ferromagnetic arrangement, the absolute value of the total magnetic moment must be reduced by $2(Z_{tot}-8)\mu_B$ from the value of Eq. (19). This rule seems valid for the Mn chalcogenides and VN, but not for the Mn pnictides, resulting in a further reduction of $2\mu_B$. In Fig. 5(a), the majority gap at E_F leaves the majority d states and GBO's fully occupied, giving a total majority occupation of 9 and then a minority occupation of 3. This electron counting yields an effective

moment of $6\mu_B$ at the central core sites. Therefore, the discrepancy may be understood from the antiferromagnetic half-metallic behavior.

As a function of bond length, the transition between ferromagnetic (FM) and antiferromagnetic (AFM) configuration takes place in several systems. This FM-AFM transition is closely related to the above-mentioned AFM half-metallic or semiconducting behavior. Since the eigenvalue-sum in general lowers the total energy when electronic states are removed from the vicinity of the Fermi energy, the half-
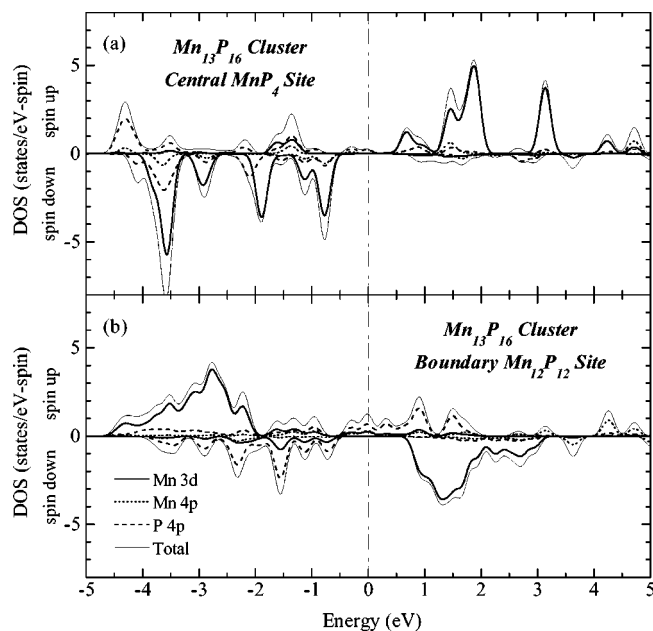
FIG. 5. Spin-resolved total and partial densities of states (DOS's) for an antiferromagnetic $Mn_{13}P_{16}$ cluster averaged at (a) central MnP_4 sites and (b) surrounding $Mn_{12}P_{12}$ sites using the GaP bond length $d_{GaP}=0.236$ nm. The central Mn atom is a spin-down state; the surrounding Mn atoms are spin-up states. The energy levels are broadened by Gaussians with a half width of 0.1 eV.
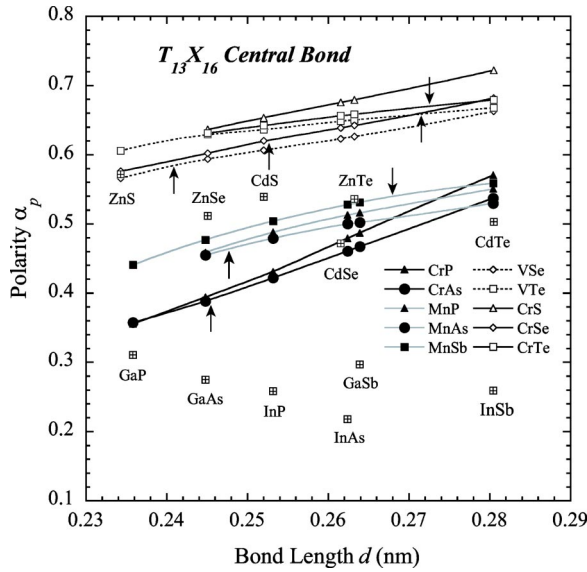
FIG. 6. Local polarity α_p of the central T-X bonds in half-metallic $T_{13}X_{16}$ clusters plotted against the bond length d used for the calculation. For each compound, the position of the equilibrium bond length predicted for the bulk system is indicated by an arrow. Several α_p values of ZB III-V and II-VI semiconductors calculated for the same cluster are also plotted.

metallic or semiconducting DOS's stabilize the AFM arrangement. In particular, FM-AFM-FM double transitions are observed in VN and VP; the AFM phase with a moment of $-13\mu_B$ appears between the FM phase with $17\mu_B$. In contrast, VS, MnS, and MnTe show AFM-FM-AFM transitions; in VS, the FM phase with $33\mu_B$ is present between the AFM phase with $-27\mu_B$, and also in MnS and MnTe, the FM phase with $59\mu_B$ is between the AFM phase with $-49\mu_B$. It is likely that the peak positions of DOS's around E_F in the metallic channel is the critical factor to determine in which configuration the result converges, FM or AFM. It should be noted that the double transitions are often accompanied by noninteger AFM magnetic moments derived from *full*-metallic DOS's. Metallic behavior indeed makes the AFM phase unstable.

V. POLARITY AND HOLE DENSITY

Although we cannot predict equilibrium bond lengths in terms of GBO's, we can directly discuss the variation of properties for any of the TX compounds under pressure. In Fig. 6, the local polarity α_p of the central T-X bond in the half-metallic $T_{13}X_{16}$ cluster is plotted against the bond length used for the calculation. Several α_p values of ZB III-V and II-VI semiconductors calculated for the same cluster are also plotted. Note that when $\alpha_p = 0.25$ for the III-V semiconductors and when $\alpha_p = 0.5$ for the II-VI semiconductors, the net charges of constituent atoms are neutral. As the polarity approaches 1, the magnitude of the net charge approaches the chemical valence. When the bond length is increased in Fig. 6, increasing polarity suggests that the T-X bond becomes more ionic. This trend arises from the decrease in the covalent energy with increasing bond length.
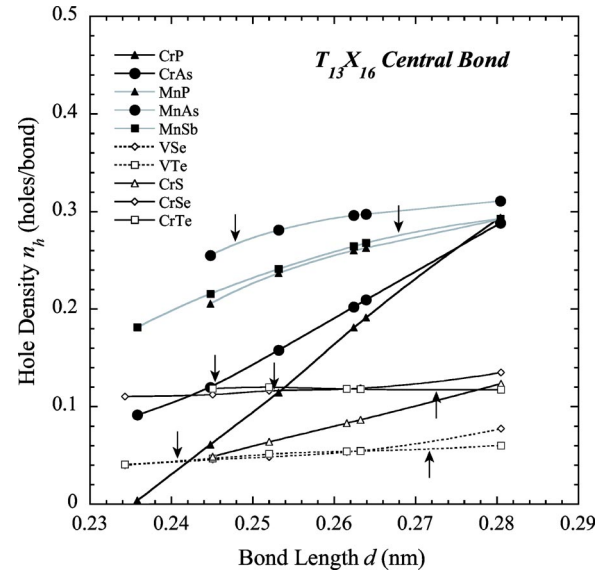
FIG. 7. Local hole density n_h of the central T-X bonds in half-metallic $T_{13}X_{16}$ clusters plotted against the bond length d used for the calculation. For each compound, the position of the equilibrium bond length predicted for the bulk system is indicated by an arrow.

As a measure of the p-d hybridization effect, the local hole density of the central T-X bond in the half-metallic $T_{13}X_{16}$ cluster is plotted against the bond length in Fig. 7. According to the ghost-bond-orbital model, the presence of holes in the majority-spin bond orbitals means the generation of the induced magnetic moment at an anion site opposite to the transition-metal moment. To evaluate the electron transfer in terms of GBO's, we will need the matrix element between a bond orbital and a t_{2g} state, $-W_2$, and half the energy change in transferring an electron from a bond orbital to a t_{2g} state, W_3. In the majority-spin channel, lowest-order perturbation theory predicts that W_2^2/W_3^2 electrons transfer from four surrounding bond orbitals to the transition-metal t_{2g} state.[44] The increase in the bond length, and the consequent decrease in the covalent energy V_2, reduces the absolute value of the second term of Eq. (6), thus pulling up the bond energy toward the fixed t_{2g} state. As a result, the absolute value of W_3 as well as W_2 is decreased with increasing bond length. Since the bond energy is relatively close to the t_{2g} state for the group-V anions, the hole density rapidly increases with the bond length. As for the group-VI anions, however, the hole density appears insensitive to the bond length. These values range from 0 to 0.3 in Fig. 7. It is evident that the ghost-bond-orbital model unambiguously defines the local polarity and the local hole density, providing a reasonable basis to understand the origin of the induced magnetic moment.

VI. NANOCLUSTER IN A MATRIX

For spintronic-device applications, half-metallic nanoclusters embedded in compound semiconductors are attracting interest. It is unclear whether the half-metallic behavior remains unaltered in the semiconductor matrix or not. The
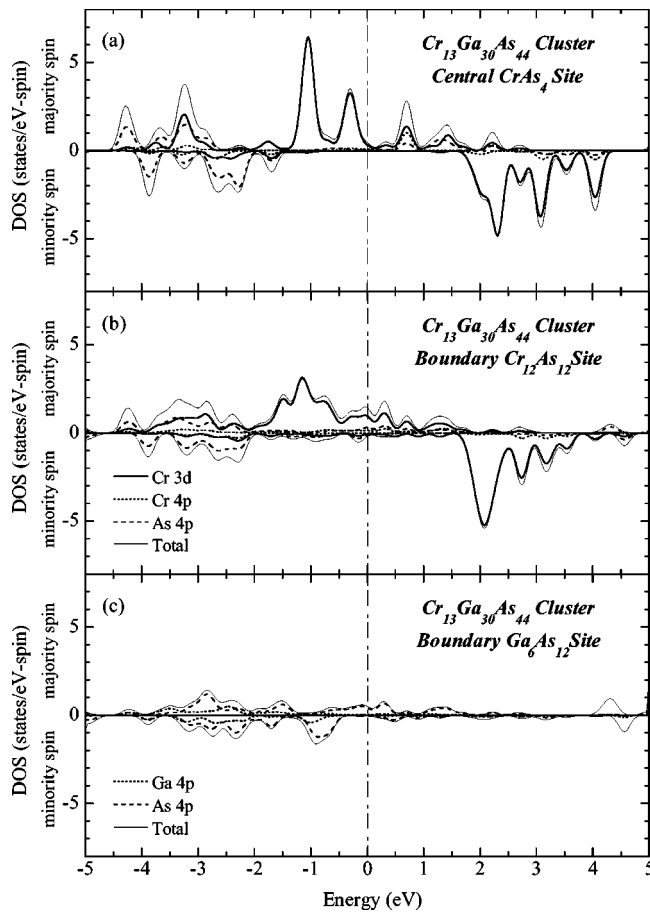
FIG. 8. Spin-resolved total and partial densities of states (DOS's) for a $Cr_{13}Ga_{30}As_{44}$ cluster averaged at (a) central $CrAs_4$ sites, (b) boundary $Cr_{12}As_{12}$ sites, and (c) Ga_6AS_{12} sites using the GaAs bond length $d_{GaAs}=0.245$ nm. The energy levels are broadened by Gaussians with a half width of 0.1 eV.

properties of heterointerfaces are of crucial importance in connection with the spin injection.

Figure 8 shows the spin-resolved total and partial DOS's for a $Cr_{13}Ga_{30}As_{44}$ cluster averaged separately at central $CrAs_4$ sites [Fig. 8(a)], boundary $Cr_{12}As_{12}$ sites [Fig. 8(b)], and Ga_6As_{12} sites [Fig. 8(c)]. The majority-spin channel is metallic in the vicinity of the CrAs-GaAs boundary sites, though a small amount of As $4p$ states appears within the minority gap in Fig. 8(b). That is, half metallicity is maintained at the CrAs-GaAs interface without any sign of interface states. Comparing with Fig. 2, we find that the surface states such as As DHS's are indeed absent in the GaAs matrix. Lattice matching prevents the appearance of dangling hybrids. This strongly suggests that the contact between the CrAs ferromagnet and the GaAs semiconductor is Ohmic and effective in injecting spins. The main source of interfacial scattering is believed to arise from the formation of a native Schottky barrier.

Figure 9 depicts the contour plot of spin-density distribution for the $Cr_{13}Ga_{30}As_{44}$ cluster in the (110) plane containing a Cr-As zigzag chain in the middle of Ga-As chains. The difference between majority- and minority-spin densities is added up for all the occupied states below E_F. The black and white truncated regions of the Cr-As chain in Fig. 9 correspond to localized magnetic moments at Cr sites and induced negative moments at As sites, respectively. They are directed opposite to each other. In the upper and lower Ga-As chains, we see that the Cr-induced moments are distributed over Ga sites as well as As sites. In fact, the induced moment varies in magnitude and direction from parallel to antiparallel with respect to the Cr moments depending on the site and even on the bond.

The total moment of the $Cr_{13}As_{16}$ cluster in GaAs is estimated to be $39.15\mu_B$, consistent with the bulk CrAs moment of $3\mu_B$ per formula unit.[24,41] Since the orbital occupations of the $Cr_{13}Ga_{30}As_{44}$ cluster are determined by the DV-$X\alpha$ cal-

(a)　　　　　　　　　　　　　　　(b)
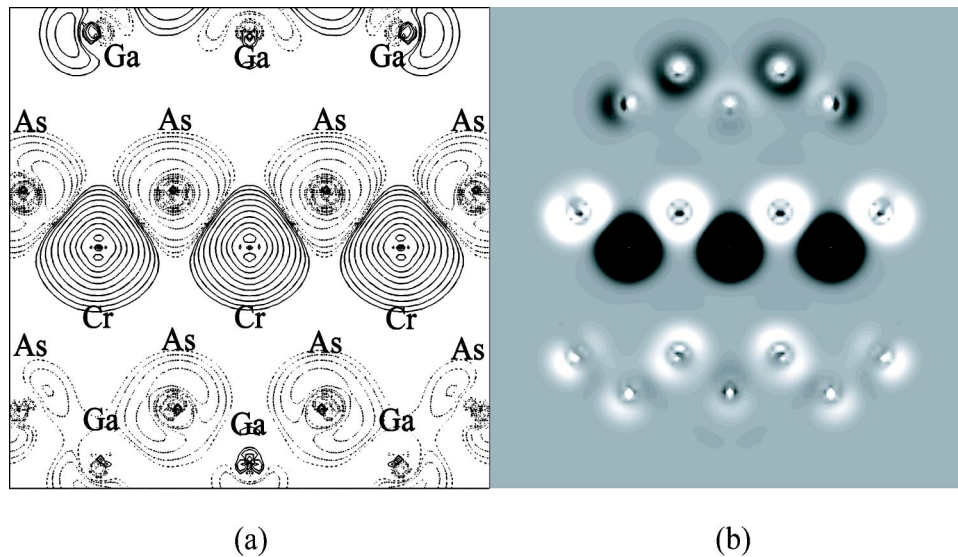
FIG. 9. (a) Contour plot and (b) gray-scale image of spin-density distribution for the $Cr_{13}Ga_{30}As_{44}$ cluster in the (110) plane containing a Cr-As zigzag chain in the middle of Ga-As chains. The difference between majority- and minority-spin densities is added up for all the occupied states below E_F. The black and white truncated regions correspond to localized magnetic moments at Cr sites and induced negative moments at As sites, respectively.

culations self-consistently, the total number of electrons in the $Cr_{13}As_{16}$ partial cluster is not necessarily an integer. The slight error from $39\mu_B$ appears to depend on the size of the whole cluster used for the calculation. We can expect the total magnetic moment of a T_kX_ℓ cluster approaches $(Z_{tot}-8)k\mu_B$ in a lattice-matched MX matrix, provided the size of the cluster model is large enough. Even when the host matrix consists of a different kind of anion (one of the same group-V or group-VI elements), the difference of the polarity will modify the induced moments but never affect the total moment as long as the half metallicity remains unaltered.

VII. CONCLUSION

The nanoclusters of ZB transition-metal pnictides and chalcogenides tend to show half-metallic behaviors with increasing bond length as well as the bulk; otherwise, the antiferromagnetic configuration characteristic of the nanocluster is stabilized. The bonding inside the nanocluster is typically covalent, indicating the formation of strong sp^3 bonds. It is convenient to employ BOM for the interpretation of the half-metallic electronic structures. The p-d hybridization effect causes the electron transfer from the bond orbitals to the d states. As a result, the holes left behind produce the induced magnetic moments at anion sites.

The Mülliken population analysis for these half-metallic nanoclusters demonstrates that the total spin magnetic moments are exact integer values depending on the numbers of both cations and anions. The crucial difference between the nanoclusters and the bulk is due to the existence of dangling sp^3 hybrids on the cluster surface. This does not severely destroy the half metallicity but modifies the total magnetic moments. The anion dangling hybrid removes $(4-\Delta Z)/4$ electrons from the d states, whereas the cation one contributes the same number of electrons to the d states.

When the nanocluster is embedded in a lattice-matched compound semiconductor with a common anion, the total magnetic moment approaches the bulk value predicted by several band calculations. The half-metallic behavior substantially remains unaltered in the semiconductor matrix. There is no sign of interface states that form a native Schottky barrier, suggesting the Ohmic nature of the contact between the nanoclusters and the compound semiconductors.

We have seen that the half-metallic nanoclusters show "digital magnetic moments." The magnetic properties depend strongly on the number and kind of constituent atoms. Besides providing new research challenges to understand the magnetic behavior, the results have enormous potential for spintronic-device applications, allowing the design of properties by control of nanostructures and heterostructures.

---

*Electronic address: mnakao@keyaki.cc.u-tokai.ac.jp

[1] G. A. Prinz, Science **282**, 1660 (1998).

[2] P. Ball, Nature (London) **404**, 918 (2000).

[3] P. Grünberg, Phys. Today **54**, 31 (2001).

[4] S. A. Wolf, D. D. Awschalom, R. A. Buhrman, J. M. Daughton, S. von Molnar, M. L. Roukes, A. Y. Chtchelkanova, and D. M. Treger, Science **294**, 1488 (2001).

[5] M. N. Baibich, J. M. Broto, A. Fert, F. N. V. Dau, F. Petroff, P. Etienne, G. Creuzet, A. Friederich, and J. Chazelas, Phys. Rev. Lett. **61**, 2472 (1988).

[6] G. Binasch, P. Grunberg, F. Saurenbach, and W. Zinn, Phys. Rev. B **39**, 4828 (1989).

[7] J. M. Kikkawa and D. D. Awschalom, Phys. Rev. Lett. **80**, 4113 (1998).

[8] J. M. Kikkawa and D. D. Awschalom, Nature (London) **397**, 139 (1998).

[9] Y. Ohno, D. K. Young, B. Beschoten, F. Matsukura, H. Ohno, and D. Awschalom, Nature (London) **402**, 790 (1999).

[10] R. Fiederling, M. Keim, G. Reuscher, W. Ossau, G. Schmidt, A. Waag, and L. W. Molenkamp, Nature (London) **402**, 787 (1999).

[11] H. J. Zhu, M. Ramsteiner, H. Kostial, M. Wassermeier, H.-P. Schonherr, and K. H. Ploog, Phys. Rev. Lett. **87**, 016601 (2001).

[12] A. T. Hanbicki, B. T. Jonker, G. Itskos, G. Kioseoglou, and A. Petrou, Appl. Phys. Lett. **80**, 1240 (2002).

[13] A. T. Hanbicki, O. M. J. van 't Erve, R. Magno, G. Kioseoglou, C. H. Li, B. T. Jonker, G. Itskos, R. Mallory, M. Yasar, and A. Petrou, Appl. Phys. Lett. **82**, 4092 (2003).

[14] V. F. Motsnyi, J. D. Boeck, J. Das, W. V. Roy, G. Borghs, E. Goovaerts, and V. I. Safarov, Appl. Phys. Lett. **81**, 265 (2002).

[15] T. Manago and H. Akinaga, Appl. Phys. Lett. **81**, 694 (2002).

[16] K. C. K. P. S. S. H. Chun, S. J. Potashnik and N. Samarth, Phys. Rev. B **66**, 100408(R) (2002).

[17] H. Ohno, J. Magn. Magn. Mater. **200**, 110 (1999).

[18] W. E. Pickett and J. S. Moodera, Phys. Today **54**, 39 (2001).

[19] R. A. de Groot, F. M. Mueller, P. G. van Engen, and K. H. J. Buschow, Phys. Rev. Lett. **50**, 2024 (1983).

[20] J.-H. Park, E. Vescovo, C. K. H.-J. Kim, R. Ramesh, and T. Venkatesan, Nature (London) **392**, 794 (1998).

[21] R. J. Soulen, Jr. *et al.*, Science **282**, 85 (1998).

[22] K. Schwarz, J. Phys. F: Met. Phys. **16**, L211 (1986).

[23] K. P. Kämper, W. Schmitt, G. Güntherodt, R. J. Gambino, and R. Ruf, Phys. Rev. Lett. **59**, 2788 (1987).

[24] H. Akinaga, T. Manago, and M. Shirai, Jpn. J. Appl. Phys., Part 2 **39**, L1118 (2000).

[25] M. Shirai, T. Ogawa, I. Kitagawa, and N. Suzuki, J. Magn. Magn. Mater. **177-181**, 1383 (1998).

[26] T. Ogawa, M. Shirai, N. Suzuki, and I. Kitagawa, J. Magn. Magn. Mater. **196-197**, 428 (1999).

[27] M. Shirai, Physica E (Amsterdam) **10**, 143 (2001).

[28] S. Sanvito and N. A. Hill, Phys. Rev. B **62**, 15553 (2000).

[29] S. Sanvito, P. Ordejon, and N. A. Hill, Phys. Rev. B **63**, 165206 (2001).

[30] S. Sanvito, G. Theurich, and N. A. Hill, J. Supercond. **15**, 85 (2002).

[31] A. Continenza, S. Picozzi, W. T. Geng, and A. J. Freeman, Phys. Rev. B **64**, 085204 (2001).

[32] Y.-J. Zhao, W. T. Geng, A. J. Freeman, and B. Delley, Phys. Rev. B **65**, 113202 (2002).

[33] I. Galanakis, Phys. Rev. B **66**, 012406 (2002).

[34] I. Galanakis and P. Mavropoulos, Phys. Rev. B **67**, 104417 (2003).

[35] A. Sakuma, J. Phys. Soc. Jpn. **71**, 2534 (2002).

[36] J. E. Pask, L. H. Yang, C. Y. Fong, W. E. Pickett, and S. Dag, Phys. Rev. B **67**, 224420 (2003).

[37] B.-G. L. Y.-Q. Xu and D. G. Pettifor, Phys. Rev. B **66**, 184435 (2002).

[38] B.-G. L. W.-H. Xie, Y.-Q. Xu and D. G. Pettifor, Phys. Rev. Lett. **91**, 037204 (2003).

[39] M. Mizuguchi, H. Akinaga, T. Manago, K. Ono, M. Oshima, and M. Shirai, J. Magn. Magn. Mater. **239**, 269 (2002).

[40] K. Ono, J. Okabayashi, M. Mizuguchi, M. Oshima, A. Fujimori, and H. Akinaga, J. Appl. Phys. **91**, 8088 (2002).

[41] J. H. Zhao, F. Matsukura, T. Takamura, D. C. E. Abe, and H. Ohno, Appl. Phys. Lett. **79**, 2776 (2001).

[42] J. H. Zhao, F. Matsukura, K. Takamura, D. Chiba, Y. Ohno, K. Ohtani, and H. Ohno, Mater. Sci. Semicond. Process. **6**, 507 (2003).

[43] W. A. Harrison, Phys. Rev. B **8**, 4487 (1973).

[44] W. A. Harrison, *Electronic Structure and the Properties of Solids* (Freeman, San Francisco, 1980).

[45] D. E. Ellis, H. Adachi, and F. W. Averill, Surf. Sci. **58**, 497 (1976).

[46] H. Adachi, M. Tsukada, and C. Satoko, J. Phys. Soc. Jpn. **45**, 875 (1978).

[47] W. A. Harrison and S. Ciraci, Phys. Rev. B **10**, 1516 (1974).

[48] R. S. Mülliken, J. Chem. Phys. **23**, 1833 (1955).

[49] R. S. Mülliken, J. Chem. Phys. **23**, 1841 (1955).

[50] The code SCAT employed in this study is available from the Society of DV-$X\alpha$ (http://www.dvxa.org/) and the CMS Forum (http://www5.plala.or.jp/double-zeta/CMS/First.html in Japanese).